ISSN 1392–1320 MATERIALS SCIENCE (MEDŽIAGOTYRA). Vol. 24, No. 2. 2018

Firing and Initiation Characteristics of Energetic Semiconductor Bridge Integrated with Varied Thickness of Al/MoO_3 Nanofilms

Peng ZHU *, Zhen GUAN, Shuai FU, Shuangfei ZHAO, Ruiqi SHEN, Yinghua YE

School of Chemical Engineering, Nanjing University of Science and Technology, Nanjing210094, China

crossref http://dx.doi.org/10.5755/j01.ms.24.2.18266

Received 28 May 2017; accepted 16 October 2017

Two types of energetic semiconductor bridges (ESCBs), with 3μm and 6μm Al/MoO_3 energetic multilayer nanofilms integrated respectively, were prepared with microfabrication technique. The influence of Al/MoO_3 nanofilms thickness on the firing and initiation characteristics of ESCBs was investigated. Results show that critical firing time and critical firing energy of ESCBs do not change significantly. The flame size of SCB-Al/MoO_3(6μm) is twice than that of SCB-Al/MoO_3(3μm) at 100μs. Furthermore, the firing duration of SCB-Al/MoO_3(6μm) is 540μs, much higher than SCB-Al/MoO_3(3μm) 300μs, which is very useful for the initiation of energetic materials. However, the contact and non-contact initiation of ESCBs on HMX-Al/MoO_3 composite explosives show that the film thickness of Al/MoO_3 has the remarkable influence on the initiation ability of ESCBs. The results from experiments deepen the understanding of the influence of thickness of Al/MoO_3 nanofilms on the firing performance of SCB, which is very meaningful for the initiation of energetic materials.

Keywords: Al/MoO_3 energetic multilayer nanofilms, energetic semiconductor bridge, firing performance, initiation performance.

1. INTRODUCTION

Semiconductor bridge (SCB) offers many potential advantages over conventional bridge wire ignition including increased safety by providing higher no-fire levels, lower firing energy, and faster response [1, 2]. Beson and co-works from Sandia National Laboratories described SCB processing and experiments evaluating SCB operation in detail [1]. They found that the SCB produces a hot plasma that ignites explosives when driven with a short (20 μs), low-energy pulse (less than 3.5 mJ). The SCB device has been used in civilian and military equipments in recent years due to its excellent performances. Nevertheless, this kind of initiator shows some limitations due to its relatively low output energy. To improve its performance, integration of nanothermite on SCB is an effective way. Energetic semiconductor bridge (ESCB) is integrated with certain thickness energetic multilayer nanofilms on SCB. Nanothermite is a metastable intermolecular composites characterized by a particle size of its main constituent, a metal and a metal oxide, under 100 nanometers. As the mass transport mechanisms that slow down the burning rates of traditional thermites are not so important at these scales, the reactions become kinetically controlled and proceed much more quickly. Different types of nanothermites have been synthesized, such as mixed or arrested milling nanopowders [3, 4], nanostructured composites [5 – 10] and multilayer nanofilms [11 – 16].

For SCB applications, multilayer nanofilms are more attracting because they can be integrated directly onto SCB with magnetron sputtering. Such solutions do provide improvement in term of reliability [17 – 20]. However, since multilayer nanofilms are highly reactive, SCB could be less safe for some applications. In order to solve the sensitive rising issue of ESCB, negative temperature coefficient thermistor chip (NTC) was integrated in parallel connection in previous work [20, 21]. After integrated with NTC, ESCB is compatible with existing firing sets used to drive SCB while withstanding electromagnetic interference and electrostatic discharge conditions.

However, there are few studies in the literature to evaluate the influence of multilayer nanofilms thickness on firing and initiation characteristics of ESCB, although this is very important for the practical applications. In this paper, two types of ESCB integrated with 3μm and 6μm Al/MoO_3 multilayer nanofilms were prepared with microfabrication technique, respectively. Firing and initiation characteristics of ESCBs were obtained by varied characterization.

2. DESIGN AND PREPARATION OF SCB-Al/MoO_3

Fig. 1 shows the schematic diagram of SCB-Al/MoO_3 chip. The device consists of six parts, namely, Si substrate (the thickness is 500 μm), SiO_2 insulating layer (the thickness is 1 μm), SCB chip made from heavily n-type doped polysilicon, Ti (30 nm)/Au (200 nm) lands, MoO_3 layer (the thickness is 150 nm, used to insulate the Al/MoO_3 films and SCB chip) and Al/MoO_3 multilayer nanofilms (the total reactive surface is 1 mm × 1 mm and the film thickness is 3 μm and 6 μm). Each bilayer consists of 30 nm Al and 45 nm MoO_3 so as to obtain a stoichiometric ratio. The resistance of SCB was designed as 1.3 ± 0.1 Ω. The SCB bridge has two V-type angles (90°) and the size is 380 μm (width) × 80 μm (length) × 2.5 μm (thickness). The SCB-Al/MoO_3 chip was

* Corresponding author. Tel.: +8615996265061.
E-mail address: *zhupeng@njust.edu.cn* (P. Zhu)

fabricated on a silicon wafer using a combination of photolithography, sputtering deposition, and lift-off techniques [19, 20].

As shown in Fig. 2, SCB-Al/MoO_3 chip was mounted into the top groove of a ceramic plug with non-conductive epoxy resin. The external diameter of the ceramic plug is 6 mm and the height is 4.5 mm. The Ti/Au lands of the SCB chip and the two pins of ceramic plug were connected together with gold wires whose diameter is 30 μm and length is 2 mm by ultrasonic bonding technology. Silver-filled conductive epoxy was used to reinforce a connection between the plug pins and the gold contact pads on SCB.

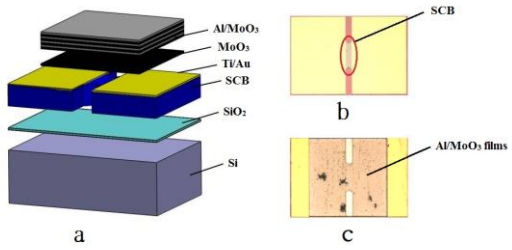

Fig. 1. a – a schematic exploded view of a SCB-Al/MoO_3 chip; b – optical image of SCB chip; c – optical image of SCB-Al/MoO_3 chip

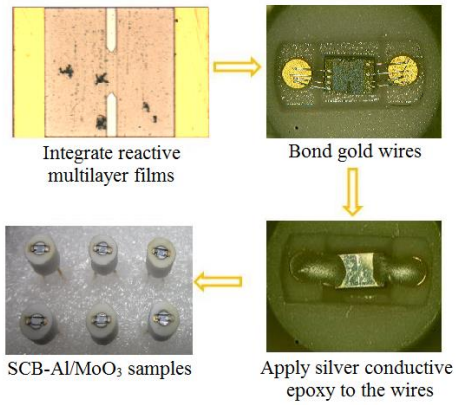

Fig. 2. Preparation schema and optical images of SCB-Al/MoO_3

3. SCB-Al/MoO_3 FIRING CHARACTERIZATION

The firing characterization was operated with a tantalum capacitor (47 μF) firing circuit as shown in Fig. 3. Voltage and current were recorded with an oscilloscope (4-channel, LeCroy44Xs) during the tests. The digital switches were adopted in the firing circuit. A high-speed camera (HG-100 K) was used to observe the initiators as electrical power was applied. In the experiment, when switch 1 was closed, the capacitor was charged by the power supply. When switch 1 was disconnected and switch 2 was closed, the SCB-Al/MoO_3 was initiated by capacitor discharging. The oscilloscope and high-speed video were triggered synchronously with the application of electrical power to the device. Multiple tests were performed with the discharge voltage ranging from 15 V to 45 V at 2.5 V increment. Under each identical condition, three samples of each kind of initiators were initiated, and then the results were averaged.

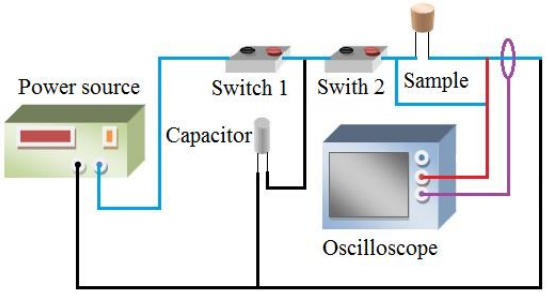

Fig. 3. Schematic drawing of the discharge circuit

3.1. Definition of firing characteristic parameters

In order to evaluate the influence of multilayer nanofilms thickness on firing performance, the characteristic parameters were defined firstly. Fig. 4 shows the variation of current, resistance and voltage along with the time under the discharge voltage in 47 μF/40 V of conventional SCB [20].

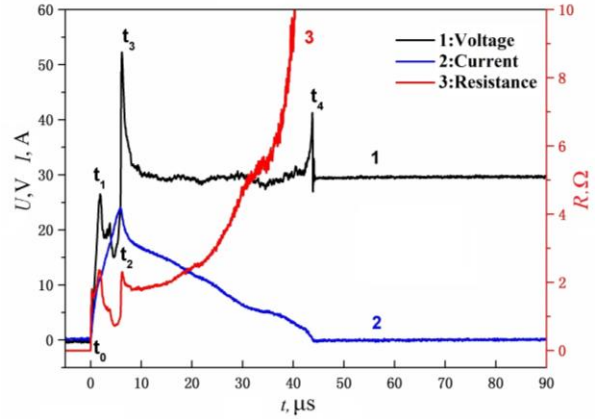

Fig. 4. Curves of current, voltage and resistance varied with time

The resistance of the bridge (get from the voltage divided by current) began to rise, which was seen with the increase of voltage across the bridge. Due to the negative temperature coefficient of SCB, whose resistance decreases roughly exponentially as their temperature increases. Once the bridge material was completely vaporized, the resistance increases promptly. The initial bump in the voltage wave was believed to be the onset of bridge melting (t_1). After that, the voltage decreased dramatically to t_2 where was believed to be the end of melting. The second sudden increase in voltage signaled the onset of the plasma where the bridge material was entirely vaporized (t_3). Because of the rapid increase in resistance during vaporizing, the current dropped off very rapidly from t_3 to the end of the current pulse (t_4). Once the bridge material was completely vaporized, the current acted to the vapor and initiated the plasma discharge. The plasma-heating course was defined as the late time discharge which covered from t_3 to t_4. Notably, t_3 is the critical point that signals the onset of the plasma where the bridge material was entirely vaporized. Therefore, this point is also called critical firing time (t_c), and its electrical energy consumption is called critical firing energy (E_c).

3.2. Comparison and analysis of the critical firing time and critical firing energy for three kinds of initiators

Fig. 5 shows the variations of critical firing time (t_c) and critical firing energy (E_c) with discharge voltage for SCB, SCB-Al/MoO_3 (3 μm) and SCB-Al/MoO_3 (6 μm). In Fig. 5 a [20, 21], E_c was obtained by numeric integration of the power vs time trace, it was calculated from the following equation. It seems that the discharge voltage has a negligible effect on E_c.

$$E_c = \int_{t_0}^{t_c} U(t) I(t) dt \,. \tag{1}$$

As shown in Fig. 5 b, t_c decreases with the potential, which is basically the same for the three samples. As well known that discharge time constant of a capacitor is within 3 τ ~ 5 τ ($\tau = RC$, R is the resistance of the initiator, C is the capacitance). The energy that the capacitor stores increases with the charging voltage rising up, so does the power applied on SCB in a certain time. Because E_c is constant, firing time decreases as the discharge voltage increases.

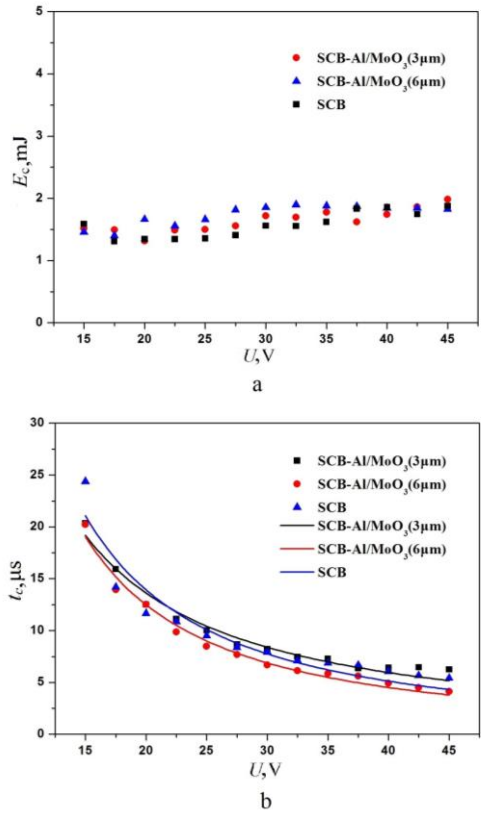

Fig. 5. Comparison of critical firing time and critical firing energy with discharge voltage: a – critical firing energy (E_c) vs Discharge voltage (U); b – critical firing time (t_c) vs Discharge voltage (U)

The results imply that t_c and E_c are only related to the size and structure of SCB in the process of electrical initiation. As far as a certain shape and size of SCB studied in this paper, it is believed that E_c is an inherent property of SCB. When the shape, size and the doping concentration of the SCB are confirmed, E_c of SCB tends to be a certain value, no matter if being covered with Al/MoO_3 films or not. Therefore, it is demonstrated that Al/MoO_3 multilayer nanofilms have no distinct influence on the t_c and E_c of SCB.

3.3. High-speed photography analysis of the firing performance

A high-speed camera was used to analysis the firing performance of the three kinds of initiators. It was set to record at 50.000 frames per second. Fig. 6 depicts the firing process of three samples discharged in 40 V. The interval between adjoining pictures is 20 μs.

As shown in Fig. 6 a, SCB heats up and melts at first. At ~ 20 μs, the plasma reaches its maximum and after that plasma becomes weaker and weaker. The whole firing process lasts for ~ 80 μs. For SCB-Al/MoO_3 (6 μm) and SCB-Al/MoO_3 (3 μm), the plasma at ~ 20 μs is almost the same. After that, plasma begins to increase and reaction between Al and MoO_3 is initiated. The violent thermite reaction gives out high temperature plasma and products. As shown in Fig. 6 b, at ~ 60 μs, SCB-Al/MoO_3 (3 μm) generates a large quantity of ejected product particles and the size of combustion flame reaches the maximum of the whole process. After that, the combustion becomes weak, and the reaction dies away. In Fig. 6 c, comparably, a fierce combustion happens and a brighter flame is generated by SCB-Al/MoO_3 (6 μm). It is believed that the flame size of SCB-Al/MoO_3 (6 μm) is twice than that of SCB-Al/MoO_3 (3 μm) at ~ 100 μs. Furthermore, the firing duration of SCB-Al/MoO_3 (6 μm) is ~ 540 μs, much higher than SCB-Al/MoO_3 (3 μm) ~ 300 μs, which is very useful for the initiation of energetic materials.

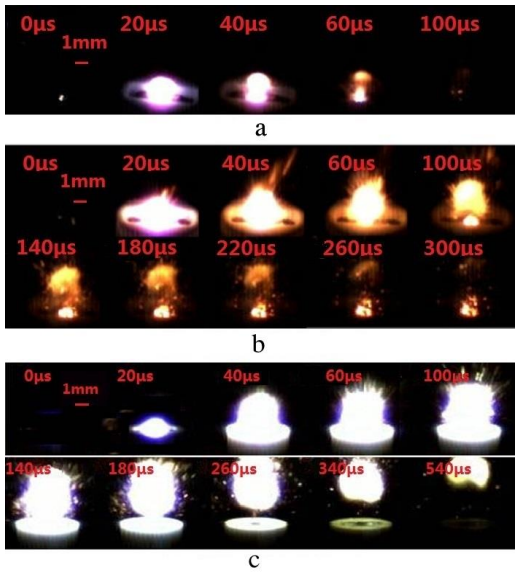

Fig. 6. High-speed images of firing process discharged in 40 V: a – SCB; b – SCB-Al/MoO_3 (3 μm); c – SCB-Al/MoO_3 (6 μm)

4. SCB-Al/MoO_3 INITIATION CHARACTERIZATION ON HMX-Al/MoO_3 COMPOSITE EXPLOSIVES

The initiation characterization of SCB-Al/MoO_3 was operated with HMX-Al/MoO_3 composite explosives. It was made of stoichiometric Al/MoO_3 nanopowders and nano-HMX, and its sensitivity could be adjusted by

varying the mass fraction of nano-HMX. Nano-Al has 50 nm average particle size, 80 wt % active metal content, and nano-MoO_3 has 100 nm average particle size with 99 wt.% purity (Aladdin Industrial Corporation, China), and nano-HMX was home-made with 300nm average particle size. For HMX-Al/MoO_3 composite explosives, after weighing the nano-HMX and Al/MoO_3 components, the mixed powders were dispersed into hexane and the suspensions were sonicated for 30 min to improve dispersibility and homogeneity. To prevent the oxidation of Al nanoparticles at elevated temperatures, the mixture was obtained by vacuum drying for 2 h at 50 °C.

In this characterization, HMX-Al/MoO_3 composite explosives were composed of 50 wt.%, 60 wt.%, 65 wt.%, and 70 wt.% fine nano-HMX particles (50 wt.%, 40 wt.%, 35 wt.%, and 30 wt.% mixed Al/MoO_3 nanopowders, respectively). Then, they were pressed into stainless charge holder (outer diameter 6 mm, inner diameter 3 mm, height 3 mm) with 20 MPa pressure. Both contact initiation and non-contact initiation were operated for better comparison.

4.1. Contact initiation of SCB-Al/MoO_3 on HMX-Al/MoO_3 composite explosives

The contact initiation device was showed in Fig. 7. It mainly consists of a SCB-Al/MoO_3 initiator, a rubber seal, six bolts closed stainless vessel and an explosion venting. It was found that HMX-Al/MoO_3 can be initiated by both SCB and ESCB when the ratio of nano-HMX is 50 wt.%, however, it becomes too insensitive to be initiated by the any of the SCB when the ratio of nano-HMX increases to 70 wt.%. Therefore, the nano-HMX at the ratio of 65 wt.% and 60 wt.% were characterized in detail, and the results are showed in Table 1. It should be noted that the discharge voltage can't exceed the upper limit of 47 μF/60 V of tantalum capacitor.

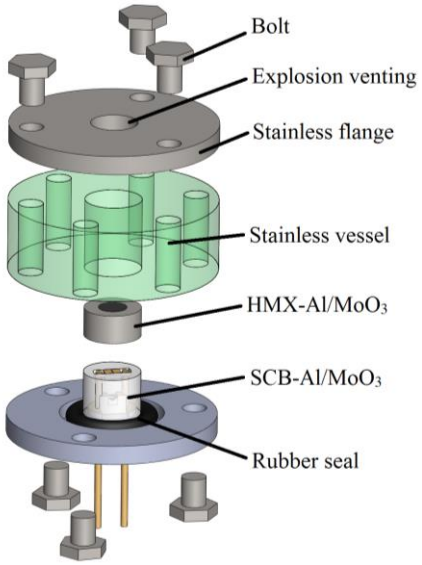

Fig. 7. Schematic diagram of the contact initiation device of HMX-Al/MoO_3

As shown in Table 1, SCB can't initiate HMX-Al/MoO_3 even discharged in 47 μF/60 V when the ratio of nano-HMX is 65 wt.%, but for SCB-Al/MoO_3 (3 μm) and SCB-Al/MoO_3 (6 μm), it is successfully to initiate HMX-Al/MoO_3 at 47 μF/24.5 V and 47 μF/17 V, respectively. Also, it is obviously that the required threshold discharge voltages decrease with the increasing film thickness. In addition, HMX-Al/MoO_3 becomes more sensitive along with nano-HMX ratio decreases to 60 wt.%, so that SCB can initiate it at 47 μF/32.5 V. In comparison, 47 μF/17 V is enough for both SCB-Al/MoO_3 (3 μm) and SCB-Al/MoO_3 (6 μm).

Table 1. Contact initiation results of HMX-Al/MoO_3 with 65 wt.% and 60 wt.% nano-HMX

Explosive	Initiator	Discharge voltage, V	Phenomenon
HMX-Al/MoO_3 (65 wt.%)	SCB	60	None fire
	SCB-Al/MoO_3 (3 μm)	24.5	fired
	SCB-Al/MoO_3 (6 μm)	17.0	fired
HMX-Al/MoO_3 (60 wt.%)	SCB	32.5	fired
	SCB-Al/MoO_3 (3 μm)	17.0	fired
	SCB-Al/MoO_3 (6 μm)	17.0	fired

4.2. Non-contact initiation of SCB-Al/MoO_3 on HMX-Al/MoO_3 composite explosives

The non-contact initiation device (Fig. 8) is almost the same as contact initiation device besides several gap rings for achieving initiation gap. A series of tests were operated to investigate the non-contact initiation ability for relatively sensitive HMX-Al/MoO_3 (60 wt.% nano-HMX). Also, it should be noted that the discharge voltage can't exceed the upper limit of 47 μF tantalum capacitor 60 V. Table 2 shows the results under the varied gaps. U 0.1 %, V, U 50 %, V and U99.9%, V represent the required discharge voltages where the initiation probabilities for HMX-Al/MoO_3 is 0.1 %, 50 % and 99.9 %, respectively. For three kinds of initiators, it is obviously that the non-contact initiation capability is enhanced greatly along with the increasing thickness of Al/MoO_3 nanofilms.

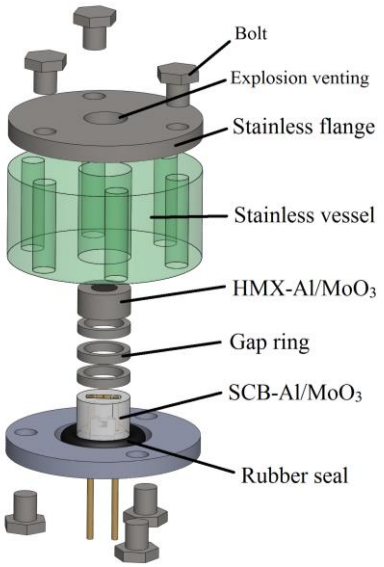

Fig. 8. Schematic diagram of the non-contact initiation device of HMX-Al/MoO_3

Table 2. Non-contact initiation results of HMX-Al/MoO_3 with 60 wt.% nano-HMX

Explosive	Initiator	Gap, mm	U0.1 %, V	U50 %, V	U99.9 %, V
HMX-Al/MoO_3	SCB	1.45	28.5	31.25	35.0
		2.45	42.5	43.75	45.0
		3.45	60.0	–	–
HMX-Al/MoO_3	SCB-Al/MoO_3 (3 μm)	8.45	15.0	17.5	20.0
		9.45	31.5	36.75	–
		10.45	60.0	–	–
HMX-Al/MoO_3	SCB-Al/MoO_3 (6 μm)	11.45	15.0	17.5	20.0
		12.45	22.5	56.5	–
		13.45	60.0	–	–

5. CONCLUSIONS

In this paper, the firing and initiation performance of SCB, SCB-Al/MoO_3 (3 μm) and SCB-Al/MoO_3 (6 μm) were studied and compared. The test results indicate the following characteristics.

1. The critical firing time (t_c) and the critical firing energy (E_c) are independent of the thickness of Al/MoO_3 films, and only related to the inherent properties of SCB.
2. The energy released by nanoscale exothermic reaction of Al/MoO_3 nanofilms enhances the plasma size and duration, which is very meaningful especially for the non-contact initiation of energetic materials.

In conclusion, the results from experiments deepen the understanding of the firing and initiation characteristics of ESCB integrated with varied thicknesses of Al/MoO_3 nanofilms.

Acknowledgments

This work was supported by the Natural Science Foundation of Jiangsu Province of China (No. BK20151486).

REFERENCES

1. **Benson, D.A., Larsen, M.E., Renlund, A.M., Trott, W.M., Bickes, R.W.** Semiconductor Bridge: A Plasma Generator for the Ignition of Explosives *Journal of Applied Physics* 62 (5) 1987: pp. 1622 – 1632. https://doi.org/10.1063/1.339586
2. **Msrtinez, M.J., Baer, M.R.** Microconvective Heating of Granular Explosives by a Semiconductor Bridge, Technical Report, 1989.
3. **Rossi, C., Zhang, K., Estève, D., Alphonse, P., Tailhades, P., Vahlas, C.** Nanoenergetic Materials for MEMS: A Review *Journal of Microelectromechanical Systems* 16 (4) 2007: pp. 919 – 931. https://doi.org/10.1109/JMEMS.2007.893519
4. **Dreizin, E.L.** Metal-based Reactive Nanomaterials *Progress in Energy and Combustion Science* 35 (2) 2009: pp. 141 – 167. https://doi.org/10.1016/j.pecs.2008.09.001
5. **Zhou, X., Torabi, M., Lu, J., Shen, R., Zhang, K.** Nanostructured Energetic Composites: Synthesis, Ignition/Combustion Modeling, and Applications *ACS Applied Materials & Interfaces* 6 (5) 2014: pp. 3058 – 3074. https://doi.org/10.1021/am4058138
6. **Zhang, K., Rossi, C., Ardila Rodriguez, G.A.** Development of a Nano-Al/CuO Based Energetic Material on Silicon Substrate *Applied Physics Letters* 91 (11) 2007: pp. 43 – H01. https://doi.org/10.1063/1.2785132
7. **Zhang, K., Yang, Y., Pun, E.Y., Shen, R.** Local and CMOS-compatible Synthesis of CuO Nanowires on a Suspended Microheater on a Silicon Substrate *Nanotechnology* 21 (22) 2010: pp. 235602 – 235608. https://doi.org/10.1088/0957-4484/21/23/235602
8. **Zhou, X., Xu, D., Zhang, Q., Lu, J., Zhang, K.** Facile Green in Situ Synthesis of Mg/CuO Core/shell Nanoenergetic Arrays with a Superior Heat-release Property and Long-term Storage Stability *Acs Applied Materials & Interfaces* 5 (13) 2013: pp. 7641 – 7646. https://doi.org/10.1021/am401955u
9. **Qiao, Z., Xu, D., Nie, F., Yang, G., Zhang, K.** Controlled Facile Synthesis, Growth Mechanism, and Exothermic Properties of Large-area Co_3O_4 Nanowalls and Nanowires on Silicon Substrates *Journal of Applied Physics* 112 (1) 2012: pp. 746 – 749. https://doi.org/10.1063/1.4731798
10. **Zhang, K., Rossi, C., Tenailleau, C., Alphonse, P.** Aligned Three-dimensional Prismlike Magnesium Nanostructures Realized onto Silicon Substrate *Applied Physics Letters* 92 (6) 2008: pp. 063123 – 063126.
11. **Rogachev, A.S.** Exothermic Reaction Waves in Multilayer Nanofilms *Russian Chemical Reviews* 77 (1) 2008: pp. 22 – 37. https://doi.org/10.1070/RC2008v077n01ABEH003748
12. **Blobaum, K.J., Reiss, M.E., Plitzko, J.M., Weihs, T.P.** Deposition and Characterization of a Self-Propagating CuOx/Al thermite Reaction In A Multilayer Foil Geometry *Journal of Applied Physics* 94 (5) 2003: pp. 2915 – 2922. https://doi.org/10.1063/1.1598296
13. **Blobaum, K.J., Wagner, A.J., Plitzko, J.M., Van Heerden, D., Fairbrother, D.H., Weihs, T.P.** Investigating the Reaction Path And Growth Kinetics in CuOx/Al Multilayer Foils *Journal of Applied Physics* 94 (5) 2003: pp. 2923 – 2929. https://doi.org/10.1063/1.1598297
14. **Petrantoni, M., Rossi, C., Salvagnac, L., Conédéra, V., Estève, A., Tenailleau, C., Alphonse, P., Chabal, Y.J.** Multilayered Al/CuO Thermite Formation by Reactive Magnetron Sputtering: Nano Versus Micro *Journal of Applied Physics* 108 (8) 2010: pp. 084323 – 084328. https://doi.org/10.1063/1.3498821
15. **Manesh, N.A., Basu, S., Kumar, R.** Experimental Flame Speed in Multi-Layered Nano-Energetic Materials *Combustion & Flame* 157 (3) 2010: pp. 476 – 480. https://doi.org/10.1016/j.combustflame.2009.07.011
16. **Manesh, N.A., Basu, S., Kumar, R.** Modeling of a Reacting Nanofilm on a Composite Substrate *Energy* 36 (3) 2011: pp. 1688 – 1697. https://doi.org/10.1016/j.energy.2010.12.061
17. **Taton, G., Lagrange, D., Conedera, V., Renaud, L., Rossi1, C.** Micro-chip Initiator Realized by Integrating Al/CuO Multilayer Nanothermite on Polymeric Membrane *Journal of Micromechanics & Microengineering* 23 (10) 2013: pp. 105009 – 105016. https://doi.org/10.1088/0960-1317/23/10/105009
18. **Zhang, K., Rossi, C., Petrantoni, M.** A Nano Initiator Realized by Integrating Al/CuO-Based Nanoenergetic Materials With a Au/Pt/Cr Microheater *Journal of Microelectromechanical Systems* 17 (4) 2008: pp. 832 – 836.
19. **Zhu, P., Shen, R., Ye, Y., Fu, S., Li, D.** Characterization of Al/CuO Nanoenergetic Multilayer Films Integrated with Semiconductor Bridge for Initiator Applications *Journal of Applied Physics* 113 (18) 2013: pp. 184505 – 184505-5. https://doi.org/10.1063/1.4804315
20. **Zhu, P., Jiao, J., Shen, R., Ye, Y., Fu, S., Li, D.** Energetic Semiconductor Bridge Device Incorporating Al/MoOx Multilayer Nanofilms and Negative Temperature Coefficient Thermistor Chip *Journal of Applied Physics* 115 (19) 2014: pp. 194502 – 194502-5. https://doi.org/10.1063/1.4876264
21. **Xu, J., Tai, Y., Ru, C., Dai, J., Shen, Y., Ye, Y., Shen, R., Fu, S.** Characteristic of Energetic Semiconductor Bridge Based on Al/MoOx Energetic Multilayer Nanofilms with Different Modulation Periods *Journal of Applied Physics* 121 (11) 2017: pp. 113301 – 11330. https://doi.org/10.1063/1.4978371